

# Probing dark energy with the next generation X-ray surveys of galaxy clusters

B. Sartoris<sup>1,2,3</sup>, S. Borgani<sup>1,3,4</sup>, P. Rosati<sup>2</sup> & J. Weller<sup>5,6,7</sup>

<sup>1</sup> *Dipartimento di Fisica, Sezione di Astronomia, Università di Trieste, Via Tiepolo 11, I-34143 Trieste, Italy*  
*e-mail: sartoris@oats.inaf.it*

<sup>2</sup> *ESO-European Southern Observatory, D-85748 Garching bei München, Germany*

<sup>3</sup> *INAF-Osservatorio Astronomico di Trieste, Via Tiepolo 11, I-34143 Trieste, Italy*

<sup>4</sup> *INFN, Sezione di Trieste, Via Valerio 2, I-34127 Trieste, Italy*

<sup>5</sup> *University Observatory, Ludwig-Maximilians University Munich, Scheinerstr. 1, 81679 Munich, Germany*

<sup>6</sup> *Excellence Cluster Universe, Boltzmannstr. 2, 85748 Garching, Germany*

<sup>7</sup> *Max-Planck-Institut für extraterrestrische Physik, Giessenbachstrasse, 85748 Garching, Germany*

11 November 2018

## ABSTRACT

We present forecasts on the capability of future wide-area high-sensitivity X-ray surveys of galaxy clusters to yield constraints on the parameters defining the Dark Energy (DE) equation of state (EoS). Our analysis is carried out for future X-ray surveys which have enough sensitivity to provide accurate measurements of X-ray mass proxies and Fe-line based redshifts for about  $2 \times 10^4$  clusters. We base our analysis on the Fisher Matrix formalism, by combining information on the cluster number counts and power spectrum, also including, for the first time in the analysis of the large scale cluster distribution, the effect of linear redshift space distortions. This study is performed with the main purpose of dissecting the cosmological information provided by geometrical and growth tests, which are both included in the analysis of number counts and clustering of galaxy clusters. We compare cosmological constraints obtained by assuming different levels of prior knowledge of the parameters which define the relation between cluster mass and X-ray observables. This comparison further demonstrates the fundamental importance of having a well calibrated observable-mass relation and, most importantly, its redshift evolution. Such a calibration can be achieved only by having at least  $\sim 10^3$  net photon counts for each cluster included in the survey, with sufficient angular resolution. We show that redshift space distortions in the power spectrum analysis carry important cosmological information also when traced with galaxy clusters. We find that the DE FoM increases by a factor of 8 when including the effect of such distortions. Besides confirming the potential that large cluster surveys have in constraining the nature of Dark Energy, our analysis emphasizes that a full exploitation of the cosmological information carried by such surveys requires not only a large statistic but also a robust measurement of the mass proxies and redshift for a significant fraction of the cluster sample, which ought to be derived from the *same* X-ray survey data. This will be possible with future X-ray surveys, such as those envisioned with the Wide Field X-ray Telescope, with an adequate combination of survey area, sensitivity and angular resolution.

## 1 INTRODUCTION

A number of independent cosmological observations, ranging from type-Ia supernovae (SNIa) (e.g. Riess et al. 2007; Perlmutter et al. 1999), to Cosmic Microwave Background (CMB) anisotropies (e.g. Komatsu et al. 2011; Larson et al. 2011) and Large Scale Structure (LSS) (e.g. Vikhlinin et al. 2009; Reid et al. 2010), convincingly show that the Universe is undergoing a phase of accelerated expansion. One of the main challenges of modern cosmology is in fact understanding the source of such acceleration. To this purpose, a number of models have been proposed that modify the two pillars of modern cosmology, general relativity and the standard model of fundamental interac-

tions (e.g. Silvestri & Trodden 2009, and references therein). Models that modify the latter and, therefore, the energy-momentum tensor in the Einstein equation are, for example, the scalar field models like quintessence (e.g. Caldwell & Kamionkowski 2009; Doran & Wetterich 2003; Zlatev et al. 1999; Ratra & Peebles 1988), k-essence (e.g. Tsujikawa 2010; Mukohyama & Randall 2004), coupled Dark Energy (e.g. Amendola 2000) and Chaplignin gas (e.g. Bento et al. 2002). Models that modify general relativity can produce the cosmic acceleration without including a Dark Energy (DE) component, but they should also satisfy stringent constraint from local (e.g. solar system) tests of gravity. Examples of such models are the braneworld models, like DGP (e.g. Dvali et al.

2000; Movahed et al. 2009),  $f(R)$  theories (e.g. Hu & Sawicki 2007; Brax et al. 2008; Appleby et al. 2010; Sofiriu & Faraoni 2010) and scalar-tensor theories (e.g. Skordis 2009).

The first model proposed to explain cosmic acceleration was based on the introduction of a cosmological constant  $\Lambda$  that can be thought as a fluid with negative pressure and equation of state (EoS) which is constant in space and time,  $p = w\rho c^2$  with  $w = -1$ . However, a cosmological constant able to drive the accelerated expansion leads to the well known problem that  $\Lambda$  needs to be so tiny with respect to any natural energy scale, that there is no theoretical justification for it. Thus, a plethora of models, characterized by different parametrizations of the DE EoS evolution, have been proposed (e.g. Wetterich 2004). In principle, it is possible to distinguish among different DE models by combining different cosmological probes, both based on the geometry of the universal background and the growth of density perturbations (e.g., Albrecht et al. 2006).

In this context, clusters of galaxies have long been recognized as potentially powerful probes of the nature of DE and cosmological models in general (e.g. Allen et al. 2011; Lombriser et al. 2010; Manera & Mota 2006, and references therein). Clusters of galaxies provide cosmological information in a number of different ways. The evolution of the cluster space density depends on cosmological parameters through both the linear growth rate of density perturbations and the redshift dependence of the volume element. The large-scale clustering of galaxy clusters is also sensitive to cosmological parameters, through the growth rate of perturbations, which affects both the bias parameter and the redshift-space distortions, as well as by sampling the shape of the underlying Dark Matter (DM) power spectrum over a broad range of wavenumbers. As of today, relatively small samples of  $\sim 100$  X-ray selected clusters, originally identified out to  $z \approx 0.8$  by the ROSAT satellite and then followed-up by *Chandra* to obtain robust mass estimates, have provided interesting DE constraints (e.g., Vikhlinin et al. 2009; Mantz et al. 2010), which complement and agree with those from CMB and SNIa observations (see also Rapetti et al. 2005). More recently, by using a complete sample of  $\lesssim 1000$  nearby clusters at  $z \lesssim 0.2$ , identified in the ROSAT All-Sky Survey (RASS; Truemper 1993), the large-scale power spectrum has been constructed over a fairly wide scale range (e.g., Balaguera-Antolínez et al. 2011).

While the first Sunyaev-Zeldovich (SZ) surveys have now started producing cluster samples of similar sizes, (e.g., Marriage & the ACT Team 2011; Williamson & the SPT Team 2011; Planck Collaboration 2011), the next generation of X-ray (e.g., eROSITA<sup>1</sup>, WFXT<sup>2</sup>) and optical (e.g., DES<sup>3</sup>, EUCLID<sup>4</sup>) surveys are expected to increase by orders of magnitude the number of galaxy clusters, further extending the redshift range over which they trace the growth of cosmic structures. Such large cluster surveys have the potential of placing very tight constraints on different classes of DE models, possibly finding signatures of departures from the standard  $\Lambda$ CDM predictions. Several studies have dealt with constraints of DE models from future cluster surveys focusing on the impact of uncertainties in cluster mass estimates (e.g. Battye & Weller 2003; Majumdar & Mohr 2004; Lima & Hu 2005, 2007; Cunha 2009; Cunha & Evrard 2010; Basilakos et al. 2010). All these analyses generally assume that,

when a cluster is detected and included in a survey, the observable (i.e., X-ray luminosity, optical richness) on which the detection is based can be related to the actual cluster mass through a suitable relation, whose functional form is assumed to be known and depends on a set of additional parameters.

A more conservative approach would instead require that for all clusters included in a survey detailed follow-up observations are carried out to calibrate suitable and robust mass proxies. Examples of such mass proxies in X-ray surveys include the total gas mass (e.g. Mantz et al. 2009) or the product of gas mass and temperature, the so-called  $Y_X$  parameter (Kravtsov et al. 2006), which can be computed when a relatively large number of photons is available. Clearly, while measuring flux for an X-ray extended source requires only  $\sim 50$  photons, or less for missions with low background, the measurement of robust mass proxies requires at least  $\sim 10^3$  photons.

In this paper, we will derive forecasts for constraints on the EoS of DE models from future X-ray surveys. We envision that these surveys will be carried out with a telescope with high-enough sensitivity to readily provide robust measurements of mass proxies and Fe-line based redshifts for  $\gtrsim 10^4$  clusters, which are all characterized by “*Chandra*-quality” data, thus avoiding the need of external and time-consuming follow-up observations. For example, the Wide Field X-ray Telescope (WFXT) concept was developed to meet such a requirement. This telescope combines large collecting area with a large field-of-view and sharp point spread function (PSF) approximately constant over the entire field of view (e.g., Giacconi et al. 2009; Murray & WFXT Team 2010; Rosati et al. 2011).

We adopt the specifications of the WFXT surveys, as an example of next generation X-ray cluster surveys, and we compute cosmological forecasts using the well-established Fisher Matrix approach (e.g., Dodelson 2003), to combine information from cluster number counts and large-scale clustering. We will quantify the constraints expected on DE models and their dependence on the knowledge of the relation between X-ray observables and cluster mass, for a range of survey strategies (i.e. depth vs. sky coverage). In the course of this study, we will discuss how number counts and the power spectrum of the large-scale distribution of clusters convey cosmological information.

As a novel contribution in this paper, we will show how the detection of Baryonic Acoustic Oscillations (BAOs) and redshift space distortions (RSDs) on cluster scales can significantly contribute to constrain cosmological parameters, similarly to a number of previous studies based on the large scale distribution of galaxies (e.g., Guzzo et al. 2008; Rassat et al. 2008; Stril et al. 2010; Wang et al. 2010).

This paper is structured as follows. In Section 2, we briefly describe the parametrizations of the DE EoS that we use, and describe our Fisher-Matrix approach for cluster number counts and power spectrum. In Section 3, we first describe the characteristics of the cluster survey, and derive the forecasts on the constraints on DE EoS parameters. In this section, we will also quantify the impact that uncertainties in the scaling relation between X-ray observables and cluster mass have on such constraints. We discuss our results and present our conclusions in Section 4.

<sup>1</sup> <http://www.mpe.mpg.de/heg/www/Projects/erosita/index.php>

<sup>2</sup> <http://www.wfxt.eu/>

<sup>3</sup> <http://www.darkenergysurvey.org/>

<sup>4</sup> <http://sci.esa.int/science-e/www/area/index.cfm?fareaid=102>

## 2 CLUSTERS AS DARK ENERGY PROBES

The relevant parameters of our analysis are the power spectrum normalization,  $\sigma_8$ , the matter density parameter,  $\Omega_m$ , and the specific parameters defining the DE EoS.

The reference analysis is carried out for the standard parametrization of the DE EoS, originally proposed by Linder (2003),

$$w(a) = w_0 + w_a(1 - a), \quad (1)$$

where  $a$  is the cosmic expansion factor (see also Chevallier & Polarski 2001). This parametrization has been used in the Dark Energy Task Force reports (DETF; Albrecht et al. 2006, 2009) to assess the constraining power of different cosmological experiments.

Albrecht et al. (2006) presented forecasts on the constraints on the  $w_0$  and  $w_a$  parameters from redshift number counts of cluster surveys. Mantz et al. (2010) derived constraints on these parameters from the observed evolution of the cluster X-ray luminosity function, using a combination of nearby clusters selected from the RASS (Truemper 1993; Ebeling et al. 1998; Böhringer et al. 2004) and medium-distant clusters selected from the (RASS based) MACS survey (e.g. Ebeling et al. 2010). An update on the constraints available at present on these parameters has been presented by Komatsu et al. (2011) using a combination of the 7-year WMAP CMB data, SN-Ia, Big-Bang Nucleosynthesis results and BAOs traced by the large-scale galaxy distribution.

Furthermore, we will also assess the constraining power of X-ray cluster surveys for the class of quintessence models, called Early Dark Energy (EDE) (Wetterich 2004). In these models, DE drives not only the accelerated expansion of the Universe at relatively low redshift, but also provides a non-negligible contribution at early times, i.e. before the last scattering surface (Doran & Wetterich 2003). A parametrization of a class of EDE models has been proposed by Wetterich (2004) as a function of the amount of DE at  $z = 0$ , the present EoS parameter,  $w_0$ , and an average value of the energy density parameter at early times,  $\Omega_{e,de}$ . The EoS parametrization that we choose is the one studied by Grossi & Springel (2009):

$$w(z) = \frac{w_0}{(1 + C \ln(1 + z))^2}. \quad (2)$$

In the above relation the quantity  $C$  is given by

$$C = \frac{3w_0}{\ln\left(\frac{1-\Omega_{e,de}}{\Omega_{e,de}}\right) + \ln\left(\frac{1-\Omega_{m,0}}{\Omega_{m,0}}\right)}, \quad (3)$$

and characterizes the redshift at which a constant EoS turns into a different behaviour according to the presence of DE at early times. Since both EDE and  $\Lambda$ CDM models have to reproduce the observed cluster abundance at low redshifts, in the EDE model we expect structures to form earlier and to have slower evolution of the halo population that in the  $\Lambda$ CDM one.

Alam et al. (2011) used the EDE parametrization by Corasaniti & Copeland (2003) to forecast constraints on these models from the abundance of X-ray clusters expected in the eROSITA survey (e.g. Predehl et al. 2007) and from the SZ power spectrum from the South Pole Telescope (SPT, Staniszewski et al. 2009). In our analysis, we use a different parametrization of EDE models, we derive forecasts for high-sensitivity X-ray surveys, and, particularly, we include the constraints from the redshift space power spectrum of clusters.

## 2.1 Cluster number counts

The information Fisher Matrix (FM) is defined as

$$F_{\alpha\beta} \equiv - \left\langle \frac{\partial^2 \ln \mathcal{L}}{\partial p_\alpha \partial p_\beta} \right\rangle, \quad (4)$$

where  $\mathcal{L}$  is the likelihood of the observable (e.g. Dodelson 2003). This can be used to understand how accurately we can estimate the value of a vector of parameters  $\mathbf{p}$  for a given model from one or more data sets, under the assumption that all parameters have a Gaussian distribution.

Following the approach of Holder et al. (2001) and Majumdar & Mohr (2003), the FM for the number of clusters,  $N_{l,m}$ , within the  $l$ -th redshift bin and  $m$ -th bin in observed mass  $M^{ob}$ , can be written as

$$F_{\alpha\beta}^N = \sum_{l,m} \frac{\partial N_{l,m}}{\partial p_\alpha} \frac{\partial N_{l,m}}{\partial p_\beta} \frac{1}{N_{l,m}}, \quad (5)$$

where the sums over  $l$  and  $m$  run over redshift and mass intervals, respectively. In this notation,  $M_{l,m=0}^{ob} = M_{thr}(z)$ , where  $M_{thr}(z)$  is defined as the threshold value of the observed mass for a cluster to be included in the survey. We write the number of clusters expected in a survey with a sky coverage  $\Delta\Omega$ , with observed mass between  $M_{l,m}^{ob}$  and  $M_{l,m+1}^{ob}$ , and observed redshift between  $z_l^{ob}$  and  $z_{l+1}^{ob}$  as

$$N_{l,m} = \Delta\Omega \int_{z_l^{ob}}^{z_{l+1}^{ob}} dz \frac{dV}{dz d\Omega} \int_{M_{l,m}^{ob}}^{M_{l,m+1}^{ob}} \frac{dM^{ob}}{M^{ob}} \int_0^\infty dM n(M, z) p(M^{ob}||M). \quad (6)$$

In the equation above,  $dV/dz$  is the cosmology-dependent comoving volume element per unity redshift interval and solid angle, and  $n(M, z)$  the halo mass function. We assume the expression provided by Jenkins et al. (2001) for the mass function of halos, with mass computed at the virial overdensity,  $\Delta_{vir} = 324$ , for the cosmological model assumed in their simulations (see their equation (B4)). We verified in test cases that all our results are left unchanged if we use instead the more recent calibration of the mass function proposed by Tinker et al. (2008). Furthermore,  $p(M^{ob}||M)$  is the probability to assign to each cluster with true mass  $M$  an observed mass  $M^{ob}$ . This probability is defined using the prescription of Lima & Hu (2005), which takes into account the presence of a lognormal-distributed intrinsic scatter in the scaling relation between observable and mass (see also Sartoris et al. 2010, S10 hereafter):

$$p(M^{ob}||M) = \frac{\exp[-x^2(M^{ob})]}{\sqrt{(2\pi\sigma_{\ln M}^2)}}, \quad (7)$$

where

$$x(M^{ob}) = \frac{\ln M^{ob} - B_M - \ln M}{\sqrt{(2\sigma_{\ln M}^2)}}. \quad (8)$$

Here  $B_M$  is the fractional value of the systematic bias in the mass estimate and  $\sigma_{\ln M}$  is the intrinsic scatter in the relation between the true and the observed mass. A negative value for  $B_M$  corresponds to a mass underestimate and, therefore, to a smaller number of clusters included in a survey, for a fixed selection function. The intrinsic scatter has the effect of increasing the number of clusters included in the survey. In fact, the number of low-mass clusters that are up-scattered above the survey mass limit is always larger than the num-

ber of rarer high-mass clusters which are down-scattered below the same mass limit (e.g., Cunha 2009, and references therein).

Including equation (7) into equation (6), we obtain

$$N_{l,m} = \frac{\Delta\Omega}{2} \int_{z_1^{ob}}^{z_{l+1}^{ob}} dz \frac{dV}{dzd\Omega} \int_0^\infty dM n(M, z) [\text{erfc}(x_m) - \text{erfc}(x_{m+1})] \quad (9)$$

where  $\text{erfc}(x)$  is the complementary error function.

In equation (9), we assume the sky coverage  $\Delta\Omega$  to be independent of the limiting mass threshold or, equivalently, of the cluster flux. This formalism can be easily generalized to include a flux-dependent sky coverage, which is due to the general degradation of resolution and sensitivity over the the field of view of X-ray telescopes. Finally, we assume that errors on the cluster redshift measurements can be ignored (see discussion in Section 3.1; see also Lima & Hu 2007 for a presentation of a method to include the effect of redshift errors in the computation of the Fisher Matrix for cluster number counts).

## 2.2 Power spectrum

A new aspect in this analysis, with respect to one presented in S10, is the inclusion of the distorted anisotropic mapping between the real space density field and measurements in redshift space caused by peculiar velocity (redshift space distortions). Following Kaiser (1987), the redshift space matter power spectrum  $\tilde{P}(k, \mu)$  in the linear regime acquires a dependence on the cosine of the angle between the wave number  $\mathbf{k}$  and the line-of-sight direction,  $\mu$ , according to

$$\tilde{P}(k, \mu, z) = (b_{eff} + f\mu^2)^2 D^2(z) P(k). \quad (10)$$

Here,  $P(k)$  is the matter power spectrum in real space,  $b_{eff}$  is the linear bias weighted by the mass function (see equation (20) in S10), and  $f(a) = d\ln D(a)/d\ln a$  is the so-called growth function, i.e. the logarithmic derivative of the linear growth rate of density perturbations,  $D(a)$ , with respect to the expansion factor  $a$ . Here we assume for the bias of halos of mass  $M$  the expression provided by Sheth & Tormen (1999).

The average cluster power spectrum calculated within a given redshift interval,  $\bar{P}_{cl}$ , can then be written as

$$\bar{P}_{l,m,i}^{cl}(\mu, k, z_l) = \frac{\int_{z_l}^{z_{l+1}} dz \frac{dV}{dz} \tilde{n}^2(z) \tilde{P}(\mu, k, z)}{\int_{z_l}^{z_{l+1}} dz \frac{dV}{dz} \tilde{n}^2(z)}, \quad (11)$$

where  $\tilde{n} = \int_0^\infty dM n(M, z) [\text{erfc}(x_m) - \text{erfc}(x_{m+1})]$ . Therefore, the Fisher Matrix for the power spectrum of galaxy clusters is

$$F_{\alpha\beta} = \frac{1}{8\pi^2} \sum_{l,m,i} \frac{\partial \ln \bar{P}_{cl}(\mu_i, k_m, z_l)}{\partial p_\alpha} \frac{\partial \ln \bar{P}_{cl}(\mu_i, k_m, z_l)}{\partial p_\beta} V_{l,m,i}^{eff} k_m^2 \Delta k \Delta \mu, \quad (12)$$

(e.g. Tegmark 1997; Feldman et al. 1994; Abramo 2011) where the sums over  $l, m, i$  run over bins in redshift, wavenumber  $k$  and angle  $\mu$ , respectively. The quantity  $V^{eff}(\mu, k, z)$  in equation (12) is the effective volume accessible by the survey at redshift  $z$ , at wavenumber  $k$  (e.g. Tegmark 1997; Sartoris et al. 2010).

For the matter power spectrum, we adopt the expression for the Cold Dark Matter provided by Eisenstein & Hu (1998), which includes the effect of BAOs. In order to quantify the information carried by the BAOs detection, we use also the power spectrum shape from Eisenstein & Hu (1998), which smoothly interpolates

through the oscillations. Moreover, we study the geometric information carried by the shape of the power spectrum by describing it with a general free parameter  $\Gamma$ , and thus ignoring its CDM specific relation  $\Gamma = \Omega_m h$ .

In our analysis, we assume the following reference values for the cosmological parameters, consistent with the WMAP-7 best fitting model (Komatsu et al. 2011):  $\Omega_m = 0.28$  for the present-day matter density parameter,  $\Omega_k = 0$  for the contribution from the curvature,  $\sigma_8 = 0.81$  for the normalization of the power spectrum,  $\Omega_b = 0.046$  for the baryon density parameter,  $H_0 = 70 \text{ km s}^{-1} \text{ Mpc}^{-1}$  for the Hubble parameter,  $n = 0.96$  for the primordial spectral index. For the DE EoS parametrization of equation (1), we take  $w_0 = -0.99$  and  $w_a = 0$  as reference values, while for the EDE model of equation (2) we assumed the reference values of  $w_0 = -0.93$  and  $\Omega_{e,de} = 2 \times 10^{-4}$ . Therefore, we have in total eight cosmological parameters, which are left free to vary in the computation of the number counts and power spectrum Fisher Matrices defined in equations (5) and (12). We note that for the above choice of the cosmological parameters, the reference DE model of equation (1) is consistent with the WMAP-7 results on CMB anisotropies. For the reference EDE model, we adopt the same values of the non-DE parameters, including  $\sigma_8$ . This implies that both models are chosen to have the same low-redshift normalization as to provide the same cluster number counts (see also Fig. 1), instead of being normalized to CMB. In the following, constraints on cosmological parameters will be shown in the  $(\Omega_m, \sigma_8)$  and  $(w_0, w_a)$  planes, while marginalizing over the remaining parameters.

Unless otherwise stated, all the constraints that we present in the following include the prior information expected from the measurement of the CMB anisotropies with the Planck experiment. This prior probability has been computed for each of the two reference DE models based on equations (1) and (2). Cosmological constraints from Planck are derived by following the description presented in the DETF Albrecht et al. (2009) and by using the method described in Rassat et al. (2008). We conservatively assume that only the 143 GHz channel will be used as science channel. This channel has beam width  $\theta_{fwhm} = 7.1$  arcmin and sensitivities  $\sigma_T = 2.2 \mu\text{K}/K$  and  $\sigma_p = 4.2 \mu\text{K}/K$ . We take  $f_{sky} = 0.80$  as the sky fraction in order to reduce the impact of galactic foregrounds. We use the minimum  $\ell$ -mode,  $\ell_{min} = 30$  in order to avoid problems with polarization foregrounds. We choose as fiducial parameters  $\theta = (\omega_m, \theta_S, \ln A_S, \omega_b, n_S, \tau)$ , where  $\theta_S$  is the angular size of the sound horizon at last scattering,  $\ln A_S$  is the logarithm of the primordial amplitude of scalar perturbations and  $\tau$  is the optical depth due to reionization. After marginalizing over the optical depth, we calculate the Planck CMB Fisher matrix in the parameters  $(\Omega_m, \Omega_{de}, h, \sigma_8, \Omega_b, \mathbf{w}, n_S)$  by using the appropriate Jacobian of the involved parameter transformation (Rassat et al. 2008). Here  $\mathbf{w}$  is a two-component vector which includes the parameters of the two DE models considered here:  $\mathbf{w} = (w_0, w_a)$  for the model of equation (1) and  $\mathbf{w} = (w_0, \Omega_{e,de})$  for the model of equation (2).

## 3 ANALYSIS AND RESULTS

### 3.1 Characteristics of the surveys

In X-ray flux-limited cluster surveys, when the cluster redshift is known, the flux limit for cluster detection can be translated into

**Table 1.** Characteristics of the envisioned WFXT surveys. Sky coverage  $\Omega$  (in sq.deg.) (Column 2). Flux limits in the [0.5-2] keV energy band (units of  $10^{-14}$  erg  $s^{-1}$   $cm^{-2}$ ) for clusters detected with  $\sim 30$  counts (Column 3, see also Giacconi et al. 2009) and with  $\geq 1500$  counts (Column 4). Number of clusters, corresponding to  $f_{1500}$ , detected at  $z > 0$  (Column 5) and  $z > 1$  (Column 6).

Survey	$\Omega$	$f_{\text{det}}$	$f_{1500}$	$N_{1500}(z > 0)$	$N_{1500}(z > 1)$
Wide	20000	0.5	15.0	8471	0
Medium	3000	0.1	3.0	8435	220
Deep	100	0.01	0.3	1509	375

a mass limit, based on a previously calibrated relation between X-ray luminosity and mass. In order to account for the uncertain knowledge of this relation, the so-called self-calibration method had been proposed by different authors (e.g. Majumdar & Mohr 2003; Lima & Hu 2005; Cunha 2009, S10). In this approach, the uncertainty in the relation between mass and observable for very large samples can be described by an intrinsic scatter and a systematic bias in the estimate of cluster masses. Thus, parameters defining the scaling relation are treated as fitting parameters to be determined along with the relevant cosmological parameters. Clearly, a more realistic and direct method to estimate cluster masses is the one adopted in Vikhlinin et al. (2009) and Mantz et al. (2010) using relatively small samples of clusters based on ROSAT data. Deep follow-up *Chandra* observations with more than  $10^3$  photons for each cluster allowed them to measure mass proxies which are closely related to cluster mass, with small ( $\lesssim 10\%$ ) intrinsic scatter. Examples of such proxies are the total gas mass,  $M_{\text{gas}}$ , calculated within a fiducial aperture radius, or the product of gas mass and temperature,  $Y_X = M_{\text{gas}} T_X$ , originally introduced by Kravtsov et al. (2006).

Next generation of cluster surveys, with high-sensitivity and good angular resolution such as WFXT, will yield large subsamples of clusters, each detected with a large enough number of photons to enable direct measurements of these mass proxies. As additional key benefit, these high quality data will allow cluster redshifts to be measured from the Fe-K 6.7 keV line in the X-ray spectra, without resorting to demanding optical spectroscopic follow-up campaigns. Yu et al. (2011) carried out a blind systematic search for K-shell and L-shell Fe line complex from *Chandra* data. Using a sample of 46 clusters in the *Chandra* archive, they found that the cluster redshift can generally be measured from X-ray data with a precision of  $\Delta z \lesssim 0.01$  when at least  $10^3$  counts are available.

In this paper, we derive cosmological forecasts for three reference WFXT surveys, which are complementary in terms of sensitivity and sky coverage: a wide survey covering 20,000 sq.deg. down to a flux in the [0.5-2] keV band of  $f_{1500} = 1.5 \times 10^{-13}$  erg  $s^{-1}$   $cm^{-2}$ , a medium survey covering an area of 3000 sq.deg. and reaching  $f_{1500} = 3 \times 10^{-14}$  erg  $s^{-1}$   $cm^{-2}$  and a deep survey over 100 sq.deg. with  $f_{1500} = 3 \times 10^{-15}$  erg  $s^{-1}$   $cm^{-2}$  (see Table 1). Given the WFXT performances (e.g. Giacconi et al. 2009), at these flux limits, clusters are detected with at least 1500 counts, thus allowing precise measurements of robust X-ray mass proxies and Fe-line based redshifts.

To convert cluster fluxes to masses, we follow the same procedure described in S10 and we refer to that paper for more details. We use the relation between X-ray luminosity and  $M_{500}$  calibrated by Maughan (2007), who analysed *Chandra* data to estimate masses from  $Y_X$  for an extended sample of clusters over the redshift range  $0.1 < z < 1.3$ .

In the following (see Sect. 3.3.1), we show the impact on cosmological constraints of setting strong priors on the parameters defining the relation between mass and X-ray observable, when at least 1500 photons per cluster are available to measure  $Y_X$  or  $M_{\text{gas}}$  proxies, as well as the cluster redshift.

### 3.2 The mass-observable relation

Besides the eight cosmological parameters, our Fisher Matrix analysis also constrains the parameters which specify the redshift dependence of the fractional mass bias,  $B_M$ , and of the intrinsic scatter  $\sigma_{\ln M}$ . Since current data and simulations (e.g. Stanek et al. 2010; Fabjan et al. 2011) show no significant evidence for a mass dependence of these parameters, in the following we do not consider this possibility. According to S10, we assume:

$$\begin{aligned} B_M(z) &= B_{M,0}(1+z)^\alpha \\ \sigma_{\ln M}(z) &= \sigma_{\ln M,0}(1+z)^\beta. \end{aligned} \quad (13)$$

In this way, we have four parameters,  $B_{M,0}$ ,  $\sigma_{\ln M,0}$ ,  $\alpha$  and  $\beta$ , which account for the uncertain knowledge in the relation between observables and mass (we refer them to hereafter as *mass parameters*). We consider a reference value  $B_{M,0} = -0.15$  for the mass bias at  $z = 0$  and  $\alpha = 0$  for its evolution. This value of  $B_{M,0}$  implies that X-ray masses are assumed to be underestimated by 15 per cent. This is in line with the level of violation of hydrostatic equilibrium found by different authors from the analysis of hydrodynamic simulations of clusters (e.g. Borgani & Kravtsov 2009, and references therein), and from the comparison between weak-lensing and X-ray masses (e.g., Mahdavi et al. 2008; Zhang et al. 2010; Okabe et al. 2010). We also assume an intrinsic scatter  $\sigma_{\ln M,0} = 0.25$ , with  $\beta = 0$  for its evolution, consistent with the  $M_{500}$ - $L_X$  relation measured by Maughan (2007). We refer to S10 for a more detailed discussion on the choice of these parameters. Following Lima & Hu (2005), we point out that we use the variance  $\sigma_{\ln M,0}^2$  and not the scatter as the varying parameter in our Fisher matrix analysis. In fact, this variance controls the excess of clusters which are up-scattered above the selection threshold, with respect to those that are down-scattered.

In summary, we have four mass parameters that add up to the eight cosmological parameters for which we compute the Fisher Matrix. In order to quantify the effect of the uncertain knowledge of the mass parameters, we set in the following four different levels of prior. In order of constraining strength, they can be described as follows.

1. *No prior*: all the four mass parameters are left free to vary by assuming no prior knowledge on their range of variation.

2. *Weak prior*: we assume  $\Delta B_{M,0} = 0.05$ ,  $\Delta\alpha = 1$ ,  $\Delta\sigma_{\ln M,0}^2 = 0.2$  and  $\Delta\beta = 1$  for the  $1\sigma$  uncertainty with which the four mass parameters are assumed to be known. The above value of  $\Delta B_{M,0}$  reflects the current uncertainty between different calibrations of violation of hydrostatic equilibrium from simulations and from the comparison of weak-lensing and X-ray masses. The reference value of  $\Delta\alpha$  allows for a large variation of the uncertainty with which we can calibrate this violation as a function of redshift. The values of  $\Delta\sigma_{\ln M,0}^2$  and  $\Delta\beta$  are rather conservative choices, in view of the large number of clusters available from future surveys which will allow an accurate estimate of the scatter in mass-observable scaling relations. We refer to S10 for a further discussion on the choice of this prior for the mass parameters.

3. *Evolution strong prior*: in order to emphasize the role played

**Table 2.** Prior on mass parameters assumed in the four cases under study (see text) and relative Figure of Merit (FoM) [see equation (14)] from the combination of three surveys. The analysis is carried out by including the Planck prior.

Reference values:	$B_{M,0} = -0.15$	$\alpha = 0$	$\sigma_{\ln M,0}^2 = (0.25)^2$	$\beta = 0$
Cases:	<i>Strong</i>	<i>Evolution</i>	<i>Weak</i>	<i>No Prior</i>
$\Delta B_{M,0}$	0	0.05	0.05	/
$\Delta \alpha$	0	0	1	/
$\Delta \sigma_{\ln M,0}^2$	0	0.2	0.2	/
$\Delta \beta$	0	0	1	/
FoM	106	91	64	61

by the uncertain redshift evolution of the mass parameters, we assume in this case the uncertainty in  $B_{M,0}$  and  $\sigma_{\ln M,0}^2$  to be the same as in the *weak prior* case, while we assume their evolution to be known to good precision, so that  $\Delta \alpha = 0$  and  $\Delta \beta = 0$ .

4. *Strong prior*: in this case we consider the uncertainties in the calibration of the mass-observable relation are so small to be neglected. While this assumption is not realistic in an X-ray cluster survey providing only detection of clusters, it is plausible for a high-sensitivity survey which provides measurements of robust mass proxies for all the clusters above the flux limits discussed in the previous section.

We summarize in Table (2) these different choices of the uncertainties in the mass parameters for the different priors that we assume.

Before proceeding with the derivation of forecasts for constraints on cosmological parameters, we verify that our fiducial cosmological models, with the above reference choice for the mass parameters, match available observational data on X-ray cluster surveys. To this purpose, we show in Fig. 1 a comparison between the predicted and the observed redshift distribution for the ROSAT Deep Cluster Survey to an X-ray flux limit of  $3 \times 10^{-14}$  erg s $^{-1}$  cm $^{-2}$  in the [0.5–2] keV band (RDCS-3, Rosati et al. 1998, 2002). We stress that this is not meant to be a fit to an observational measurement of the cluster abundance up to  $z \sim 1$ , but rather a test that our reference model is consistent with current observations. The redshift distributions for the two reference DE models have been obtained by convolving the predicted redshift distributions with the flux-dependent RDCS sky coverage, which provides complete information on the survey selection function. We adopt a minimum luminosity of  $L_X[0.5 - 2\text{keV}] = 10^{42}$  erg/s which is appropriate for the RDCS selection function.

The good agreement with the data indicates that our reference model can be used to provide a realistic extrapolation of the evolution of the cluster mass function over redshift and mass ranges that are not probed by currently available data.

In Fig. 2 and 3, we show the cumulative redshift distributions of clusters to be observed in the Wide, the Medium and the Deep surveys according to our reference DE and EDE models, respectively. In the lower panel of Fig. 3, we also show the ratio between the cumulative redshift distributions obtained for these two DE models by combining the three surveys. In order to reproduce the observed abundance of clusters at low redshift, in EDE models structures start to form earlier and the halo population follows a slower evolution than in the  $\Lambda$ CDM prescription. We note that the combination of the three surveys would provide about  $2 \times 10^4$

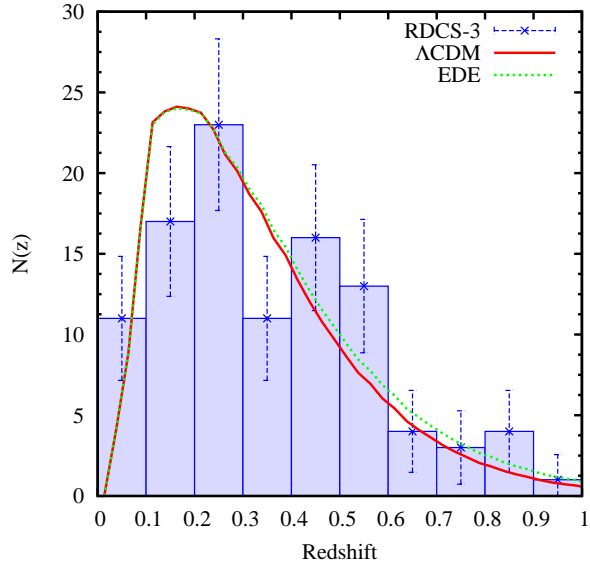


**Figure 1.** Comparison between the observed redshift distribution of X-ray selected galaxy clusters (histogram with symbols and errorbars) from the ROSAT Deep Cluster Survey -3 (Rosati et al. 2002, 1998) and predictions from the reference DE model based on equation (1) (red solid curve) and EDE model of equation (2) (green dotted curve). Errorbars on observational data points correspond to  $1\sigma$  Poissonian uncertainties (Gehrels 1986).

clusters with sufficient photons to allow robust measurements of X-ray mass proxies. The total number of clusters is dominated by the Wide and the Medium surveys. The Deep survey is expected to provide a smaller number of clusters at low redshift, due to the smaller survey area. However, the number of distant clusters at  $z > 1$  is dominated by the Deep survey, owing to its higher sensitivity (see also S10).

### 3.3 Cosmological constraints

Having defined the reference cosmological model and the characteristics of the X-ray cluster surveys, we present in this section forecasts on constraints of DE EoS parameters. We show our results in terms of constraints on the  $(\Omega_m, \sigma_8)$  and the  $(w_0, w_a)$  plane at the 68 per cent confidence level, after marginalizing over the other cosmological and mass parameters, and in terms of Figure of Merit (FoM). The concept of FoM for DE constraints was introduced in the Dark Energy Task Force (DETF) report (e.g., Albrecht et al. 2009) in order to quantify the knowledge on DE EoS parameters that future cosmological experiments can reach. In general, the FoM for the capability of an experiment to constrain a pair of cosmological parameters  $(p_i, p_j)$  can be defined as

$$\text{FoM} = \left( \det \left[ \text{Cov}(p_i, p_j) \right] \right)^{-1/2}, \quad (14)$$

where  $\text{Cov}(p_i, p_j)$  is the covariance matrix between the two interesting parameters. With this definition, the FoM is proportional to the inverse of the area encompassed by the ellipse representing the 68 per cent confidence level for model exclusion.

In the computation of the cluster number counts Fisher Matrix, equation (5),  $N_{l,n}$  is calculated within intervals of observed redshift,

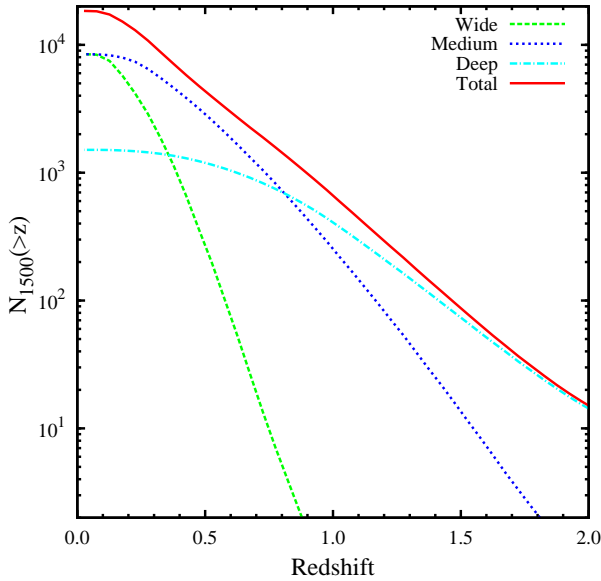


**Figure 2.** The cumulative redshift distributions of clusters detected with more than 1500 net counts in the three surveys, as predicted by the reference DE model of equation (1). Dashed (green), dotted (blue) and dot-dashed (cyan) curves are for the Wide, Medium and Deep WFXT surveys, respectively, while the solid (red) curve represents the sum of the three.

with width  $\Delta z = 0.05$  out to  $z_{max} = 2$ . As for the observed mass, we use bins of width  $\Delta \log M = 0.01$ , extending from the lowest mass limit determined by the survey selection function at a given redshift, up to  $10^{16} h^{-1} M_{\odot}$ . We have verified that with this tight binning in mass we saturate information provided by cluster number counts to constrain cosmological and mass parameters.

In the computation of the power spectrum Fisher Matrix, given by equation (12), the average cluster power spectrum defined by equation (11) is calculated by integrating over redshift intervals having constant width  $\Delta z = 0.2$ . This binning, which is coarser than the one adopted for the number counts, was chosen as a compromise between the need of extracting the maximum amount of information from clustering evolution and the request of limiting the covariance between adjacent  $z$ -intervals (e.g., Stril et al. 2010). Indeed, the contribution from different  $z$ -bins can be added in Fisher Matrix defined by equation (12) only if they carry statistically independent information. Using small redshift bins implies that the neighbouring bins are significantly correlated. In this case, the covariance terms between different redshift intervals should be included in the likelihood function entering in the expression of equation (12) for the power spectrum FM. As for the wave number, we consider a minimum value of  $k = 0.001 \text{ Mpc}^{-1}$ ; the choice of this minimum value does not change the final results, because extremely large wave modes are not sampled by the surveys used and, therefore, do not provide any contribution to the Fisher Matrix. The maximum value chosen is  $k_{max} = 0.3 \text{ Mpc}^{-1}$ . This choice derives from the need to maximize the information extracted from the three surveys, while avoiding at the same time the contribution from small-scale modes where the validity of the linear bias model is compromised by the onset of non-linearity (e.g. Percival & White 2009; Stril et al. 2010; Rassat et al. 2008, see also S10 for a quantitative analysis of the dependence on

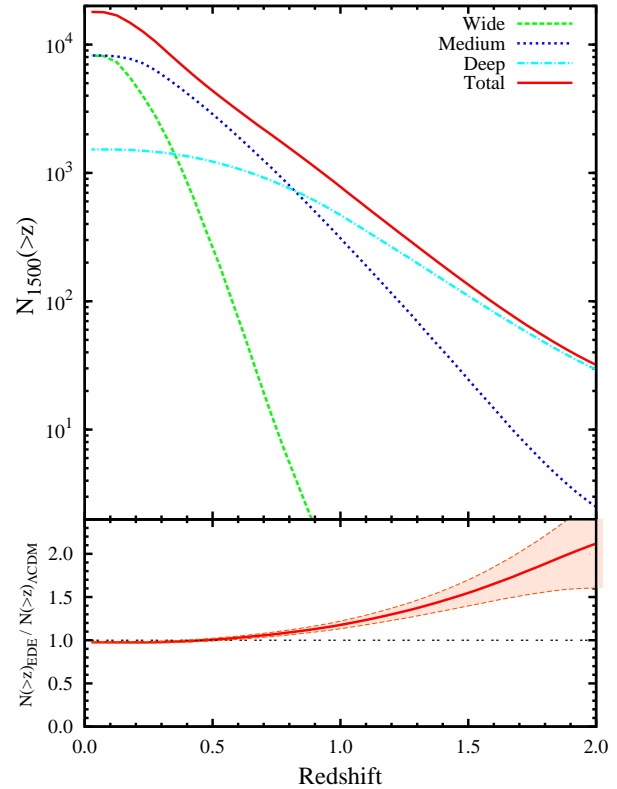


**Figure 3.** The cumulative redshift distributions of clusters detected with more than 1500 net counts in the three surveys, as predicted by the reference EDE model of equation (2). Dashed (green), dotted (blue) and dot-dashed (cyan) curves are for the Wide, Medium and Deep WFXT surveys, respectively, while the solid (red) curve represents the sum of the three. In the bottom panel we show the ratio between the cumulative redshifts distributions for the combined survey, as predicted by the reference EDE model and the reference DE model shown in Fig. 2. The shaded region represents the Poissonian error on this ratio.

$k_{max}$  of FM constraints for non-Gaussian models). In particular, Crocce & Scoccimarro (2008) studied the non-linear evolution of BAOs in the Dark Matter power spectrum and correlation function. They showed that at  $k = 0.18 \text{ Mpc}^{-1}$  the power spectrum predicted by the linear theory is lower by a factor of 1.2 at  $z = 0$  with respect to the non-linear power spectrum. However, we stress that the contribution of information to the Fisher Matrix carried by the power spectrum at different redshifts decreases for both very high and very low values of  $k$  (Sartoris et al. 2010). The contribution of the power spectrum directly depends on the effective volume, ( $V_{eff}$  in equation 12). This quantity depends on the power spectrum itself, which is set by the bias parameter, and on the level of Poisson noise, which is set by the number density of clusters and is maximized at  $k \approx 0.01 \text{ Mpc}^{-1}$  (see Fig.7 of S10).

Wavenumber bins have been chosen to have log uniform width  $\Delta \log k = 0.1$ . Lastly, introducing redshift space distortions information, the power spectrum acquires a dependence on  $\mu$ , which is defined as the cosine of the angle that  $\mathbf{k}$  makes with the line of sight (equation (10)). This implies that the Fisher Matrix also involves a sum on  $\mu$  that runs from  $\mu = -1$  to  $\mu = 1$ . We choose to divide the interval of  $\mu$  into 9 bins. An odd number of bins is required so that the central bin samples the values of the redshift space power spectrum computed for  $\mu = 0$ . In fact, this number of bins maximizes the power spectrum at different redshifts

**Table 3.** Figure of Merit and r.m.s. uncertainty in the DE EoS parameters, for the WFXT three surveys, and for their combination. The analysis is carried out by including the Planck prior and assuming *strong prior* for the mass parameters.

Surveys	Deep	Medium	Wide	Total
FoM	20	60	17	106
$\sigma_{w_0}$	0.20	0.097	0.14	0.064
$\sigma_{w_a}$	0.94	0.54	0.70	0.41

and wavenumbers and, therefore, the contribution of  $V_{eff}$  (Eq.12) to the Fisher Matrix. We also verified that a larger number of bins does not tighten constraints from the redshift space distortions.

The results of our analysis are presented in Fig. 4 where we plot the 68 per cent confidence levels on the  $(\Omega_m, \sigma_8)$  and  $(w_0, w_a)$  plane, in the left and right panels, respectively. In each panel, we show the contours obtained for each of the three surveys and for their combination. Contours are all obtained by combining information from number counts and power spectrum, also including the prior information from Planck. A *strong prior* is also assumed for the knowledge of the mass parameters (see Section 3.2).

The results in Fig. 4 show the trade-off between surveys area and depth in constraining different cosmological parameters. As for the results on  $(\Omega_m, \sigma_8)$ , there is no continuous trend in the constraining power of the three surveys as we reduce the covered area and increase sensitivity. The Medium Survey is in fact the one with most constraining power, especially for  $\sigma_8$ , while the Deep and the Wide Surveys are somewhat less constraining. Furthermore, the three surveys provide comparable constraints on  $\Omega_m$ . This is consistent with the expectation that constraints on this parameter are mainly provided by information on the CMB anisotropies, carried by the Planck prior. As for  $\sigma_8$ , we remind that this parameter determines the timing of structure formation, therefore, constraints on its value are sensitive to both the number of massive clusters included in a survey, and on the effective redshift range covered by the survey itself. In this respect, the Medium Survey provides the best compromise between the number of massive clusters detected within its area and depth.

As for the constraints on  $(w_0, w_a)$ , we note that their dependence on the survey area/depth is different from the case of the  $(\Omega_m, \sigma_8)$  parameters. While the Medium survey is still the most constraining one, we note that the Deep Survey predict a tighter degeneracy between  $w_0$  and  $w_a$  than the Wide survey. This translates into tighter constraints on the redshift evolution of the DE EoS, if a prior knowledge on  $w_0$  is available, consistent with the fact that the Deep Survey covers a larger redshift interval and provides the larger amount of clusters for redshift greater than 0.9. This example illustrates that the choice of the survey strategy depends in principle on the cosmological parameters that one is mostly interested in. In Table (3) we report the values of the FoM and the r.m.s. uncertainty in the DE EoS parameters for each survey and for their combination, after marginalizing over the other parameters. The values of the FoM in this table confirm that Medium Survey alone carries most of the contribution to the FoM obtained by combining the three surveys.

### 3.3.1 Effect of mass parameter priors

As a first test, we present the effect that using progressively stronger priors on the mass parameters has on cosmological constraints. The

results of this analysis are shown in Fig. 5, where we plot the constraints on cosmological parameters obtained by combining information from cluster number counts and power spectrum, from the three surveys together. The Fisher Matrix from the cluster experiment is also combined with the Planck Fisher Matrix.

In the left panel of Fig. 5, we show the constraints in the  $(\Omega_m, \sigma_8)$  plane. A progressively better knowledge of the relation between X-ray observable and cluster mass turns into progressively tighter constraints on the  $\sigma_8$  parameter, while leaving the results on  $\Omega_m$  basically unchanged. The reason for this behaviour is that constraints on  $\Omega_m$  are mainly determined by the measurement of the CMB anisotropies and by the shape of power spectrum, which however only provide rather loose constraints on  $\sigma_8$ . On the other hand, the power spectrum normalization is determined by the growth of cosmic structures, which is traced by the evolution of the halo mass function. Since a precise measurement of the mass function can only be obtained through a detailed knowledge of the mass parameters, it is of little surprise that such parameters determine the accuracy with which  $\sigma_8$  can be measured.

As for the constraints on the DE EoS parameters (see right panel of Fig. 5), we note that improving the knowledge of the mass parameters from the *no prior* (red ellipse) to the *weak prior* (cyan ellipse) case only brings a modest enhancement of the constraining power of the surveys. The main reason for this is that constraints on DE parameters are here mainly contributed by the evolution of linear perturbation growth. On the other hand, constraints on the growth are rather degenerate with the uncertainty in the redshift evolution of the mass parameters, which is assumed to be rather generous also in the *weak prior* case. Indeed, a more significant improvement in the constraints on the DE parameters is obtained for the *evolution strong prior* case (blue ellipse), which assumes a precise knowledge of the parameters determining the evolution of the mass-observable relation, with only a slight further improvement in the constraints obtained for the *strong prior* case (green ellipse). These results confirm the importance of accurately calibrating the evolution of the scatter and bias parameters by measuring different mass proxies in high redshift clusters selected in the Deep survey. Indeed covering at a high sensitivity an even small sky area allows one to obtain a robust calibration of the scaling relations between the cluster mass and X-ray mass proxies over a large redshift baseline. As shown in Fig. 2, this survey will provide about 400 clusters at  $z > 1$  for which measurements of redshift,  $M_{gas}$  and  $Y_X$  will be possible, out of which about 100 are expected to lie at  $z > 1.5$ . In Table 2, by showing the value of the FoM obtained, we summarize the results obtained in our analysis on the effect of uncertainties on the mass parameters in the determination of DE EoS parameters.

### 3.3.2 Combining cluster number counts and power spectrum

We discuss now how the combination of number counts and power spectrum information enhances cosmological constraints. To this aim, we show the improvement on constraints obtained by adding progressively information from the cluster number counts, the mean cluster power spectrum analysis and the CMB prior from Planck. The results are presented in Fig. 6 in the  $(\Omega_m, \sigma_8)$  (left panel) and  $(w_0, w_a)$  planes. Constraints are obtained by combining information from the three surveys together and assuming *strong prior* on mass parameters. The redshift evolution of the cluster number counts sets the direction of degeneracy for the constraints on  $\Omega_m$  and  $\sigma_8$ . Such constraints are mainly placed on the linear growth factor of density perturbations through the mass function. Furthermore, since the density parameters contributed by matter

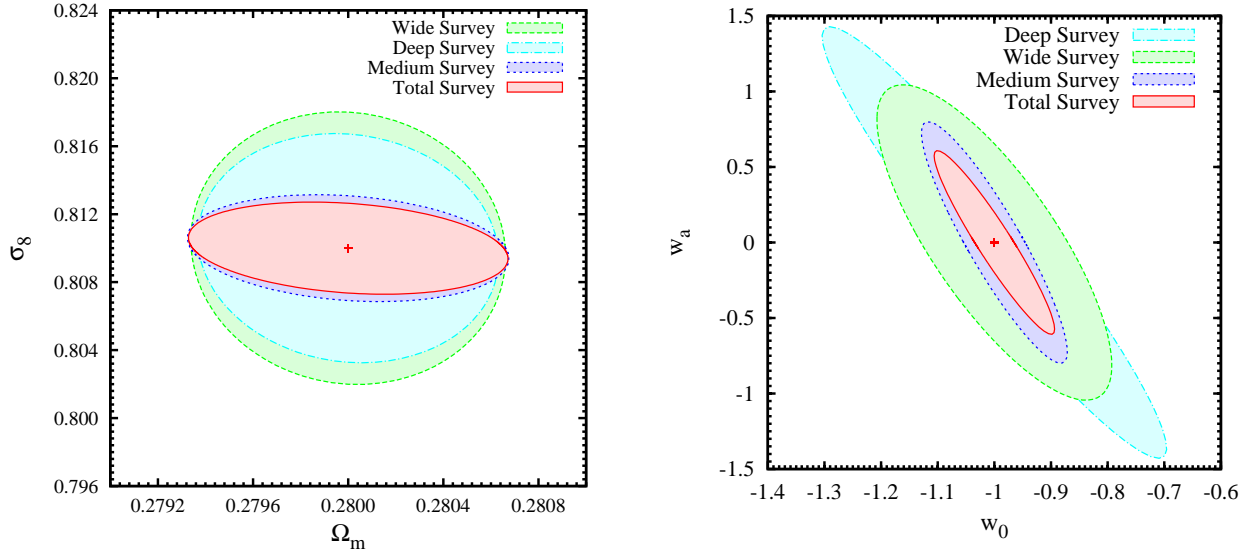


**Figure 4.** Constraints at the 68 per cent confidence level on the  $(\Omega_m, \sigma_8)$  parameters (left panel) and on the  $(w_0, w_a)$  DE parameters (right panel). In each panel, forecasts for the Deep, Medium and Wide WFXT cluster surveys are shown with the cyan, blue and green ellipses, respectively, by combining number counts and power spectrum information. The red ellipse are the constraints obtained from the combination of the three surveys. All constraints are obtained by assuming a *strong prior* on the knowledge of the mass parameters and combining the Fisher Matrices for cluster number counts, cluster power spectrum and CMB Planck experiment.

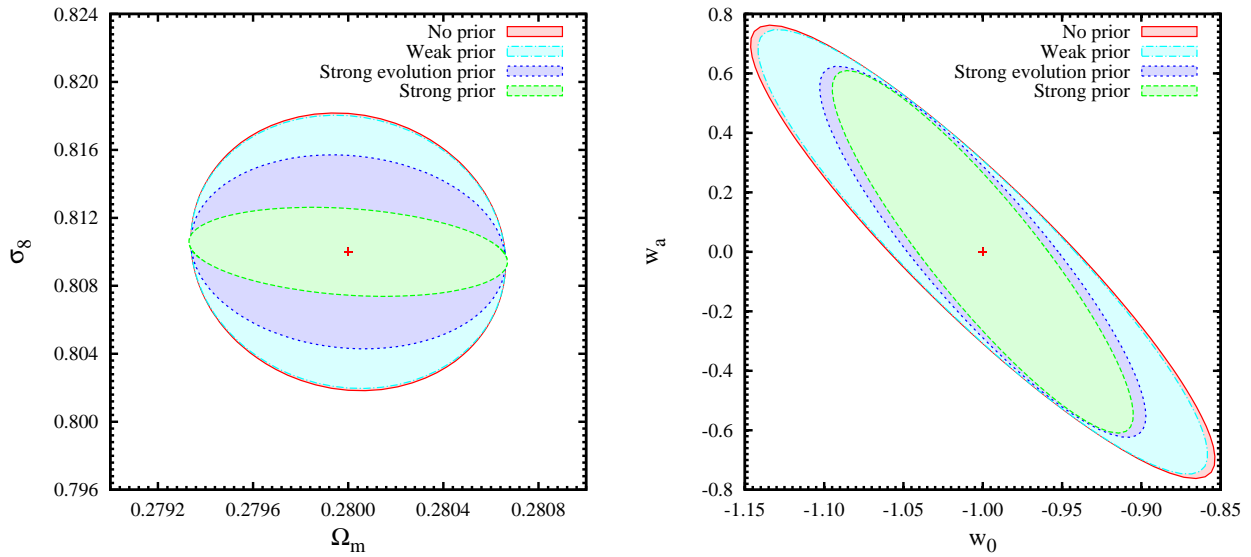


**Figure 5.** Constraints at the 68 per cent confidence level on the  $(\Omega_m, \sigma_8)$  (left panel) and on the  $(w_0, w_a)$  (right panel) planes. Different ellipses correspond to different assumptions on the prior for the mass parameters (see text): *no prior* case (red), *weak prior* case (cyan), *evolution strong prior* case (blue), and *strong prior* (green). All constraints are obtained by combining cluster number counts and power spectrum information for the combination of the three surveys.

and DE also affect the expansion history of the Universe, we expect their values to be constrained by the cluster number counts, through the redshift evolution of the comoving volume element. The power spectrum analysis provides information on the growth rate of cosmic structure through the bias factor, and the RSDs effect. Moreover BAO features, that depend on the expansion history of the universe (see Section 3.3.3), and the power spectrum shape (see Section 3.3.4) are also sensitive to the underlying DM distribution.

In Fig. (6), we show that adding the power spectrum information to the number counts substantially shrinks the contours. Including the information from the Planck prior (red contour) further contribute to tighten the contours in the  $(\Omega_m, \sigma_8)$  plane. In order to verify whether CMB add information only by constraining the curvature of the Universe, we also show with the green contour the effect of assuming instead a flat Universe on the cluster constraints. In this case, results on  $(\Omega_m, \sigma_8)$  are not drastically improved with respect to the case in which curvature is a free parameter, while they are significantly worse than with the Planck prior. The reason for this result is that CMB anisotropies provide constraints not only on the curvature, but also on the Hubble parameter  $h$ , on  $\Omega_b$  and on the primordial spectral index  $n_s$ . All these parameters enter in defining the shape of the power spectrum, along with  $\Omega_m$ . Therefore, their precise determination from the CMB turns into a significant improvement of constraints on the density parameter from the shape of the power spectrum.

As for the constraints on  $(w_0, w_a)$ , their direction of degeneracy changes as a specific geometry is assumed. Imposing the flat prior corresponds to fix the redshift at which DE component,  $\Omega_{de}$ , starts dominating over  $\Omega_m$  and, therefore, breaks the degeneracy between  $w_0$  and  $w_a$ . By including the Planck prior, instead of assuming flatness, has a smaller impact than for the  $(\Omega_m, \sigma_8)$  constraints. Therefore, even though CMB alone does not provide in itself stringent constraints on the DE EoS, it is quite effective in improving the corresponding constraints from cluster number counts and power spectrum, owing to its leverage on the geometry of the Universe. The Deep and Medium surveys dominate the cluster counts at  $z \gtrsim 0.4$  (see Fig. 2), thus improving the constraints on the growth rate of perturbations in a redshift range where it is sensitive to the DE EoS.

### 3.3.3 Information from Baryonic Acoustic Oscillations

We quantify now the geometrical information brought by the presence of BAOs features in the matter power spectrum. BAOs appear as wiggles superposed on the power spectrum of the dominant Dark Matter component (e.g. Eisenstein & Hu 1998). The oscillation scale is proportional to the inverse of the sound horizon at the matter radiation equivalence. BAOs carry at lower redshift the same information that baryonic oscillations in the CMB photon power spectrum provide at the last-scattering redshift. The position of the wiggles is related to the amount of dark matter and baryons. As  $\Omega_m h^2$  increases, the first peak is shifted to higher  $k$  values and, moreover, the valleys and peaks become slightly narrower. The amplitude of the wiggles also depends on  $\Omega_b$  as the oscillations grow stronger as the baryon fraction increases. In this analysis, we study the constraints on the  $(w_0, w_a)$  DE EoS parameters as obtained by using the transfer function by Eisenstein & Hu (1998), which includes BAOs, and by using instead the transfer function that smoothly interpolates through the oscillations (see equation (30) of Eisenstein & Hu 1998). In the latter case, the presence of

baryons manifests itself only by modifying the overall shape of the transfer function.

We carried out the analysis including and excluding BAOs in the shape of the matter power spectrum used to compute cluster number counts and bias. In order to better appreciate the information carried by BAOs, in both cases we do not assume any prior on cosmological parameters, while we use *strong prior* on the mass parameters. As expected, constraints from Wide survey are those that benefits most from the presence of the BAOs. This is mainly due to the fact that this survey provides the best sampling of the long wavelength modes corresponding to the most prominent first oscillation harmonics. The inclusion of the BAOs analysis increases the FoM by a factor of 2.1 in this case. On the other hand, no significant information on BAOs is provided by the Medium and the Deep surveys. The FoM from the Medium survey does not increase, while the FoM provided by Deep survey increases by a factor of 1.2. In fact, the Deep survey seems to convey slightly more information on the BAOs. This is mainly due to the higher number density of clusters in this survey, which reduces the noise when sampling the BAOs.

### 3.3.4 Information from the power spectrum shape

To quantify the geometrical information encoded in the matter power spectrum shape, we fit the shape parameter  $\Gamma$  in our analysis, regardless of its dependence on  $\Omega_m$ ,  $h$  and  $\Omega_b$  which is specific to the type of Dark Matter. We compare the results obtained by assuming Dark Matter to be Cold with those obtained for a general form of Dark Matter. In the latter case  $\Gamma$  is treated as a free parameter. In the former, under the CDM assumption, the shape of the transfer function is given by  $\Omega_m h$ , that specifies the size of the horizon at the equality epoch, and by the baryon density parameter. For this reason, the power spectrum shape carries information on the cosmic expansion history. Relaxing the CDM assumption, other characteristic scales could affect the shape of the power spectrum. For instance, if massive neutrinos provide a contribution to the DM budget, the power spectrum is expected to be suppressed with respect to the pure CDM scale on scales smaller than the characteristic neutrino free streaming scale (e.g., Hannestad 2010; Marulli et al. 2011). Already available data on the evolution of the cluster mass function have been used to set interesting constraints on neutrino mass (Mantz et al. 2010).

In Fig. 7, we show the expected 68 per cent confidence ellipse on the  $(\Omega_m, \sigma_8)$  plane, by combining cluster number counts and power spectrum information for the three surveys together, when leaving the shape  $\Gamma$  as a free parameter (blue dotted ellipse) and when using instead its CDM expression (red solid ellipse). In order to elucidate the effect of a preadopted CDM power spectrum on these constraints, we fix to their reference values the parameters that, along with  $\Omega_m$ , determine the power spectrum shape, namely  $\Omega_b$ , the Hubble parameter  $h$  and the primordial spectral index  $n_s$ . By removing the assumption of a CDM spectrum constraints become weaker. In addition, since the effect is more pronounced for the matter density parameter, the direction of degeneracy changes in the sense of a milder dependence of  $\sigma_8$  on  $\Omega_m$ .

The shape of the power spectrum is better sampled by the largest survey area covering the widest range of scale. This translates into a stronger constraint on the  $\Omega_m$  parameters and consequently on the DE EoS parameters. Thus, if we relax the assumption of CDM for the shape of the power spectrum, the FoM of the Wide survey decreases by 7 per cent. This decrement is less pronounced in the Medium and Deep surveys, whose FoM decreases

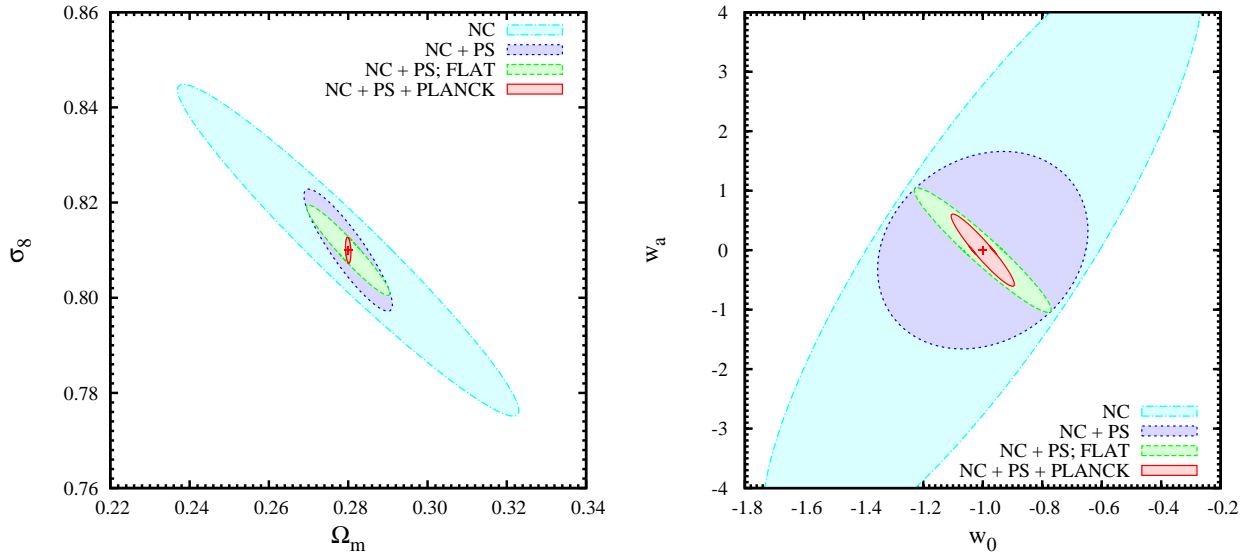


**Figure 6.** Constraints at the 68 per cent confidence level on the  $(\Omega_m, \sigma_8)$  parameters (left panel) and on the  $(w_0, w_a)$  DE EoS parameters (right panel). Contours, in order of decreasing area, are obtained by including the Fisher Matrix from cluster number counts only (cyan ellipse), adding cluster power spectrum information (blue ellipse), further assuming a flat Universe (green ellipse) and adding priors from the Planck experiment while leaving geometry free (red ellipse). All constraints are obtained by combining information from the three surveys and assuming the *strong prior* on the mass parameters.

respectively by 4 and 5 per cent, owing to their weaker sensitivity to the spectrum shape.

### 3.3.5 Information from redshift-space distortions

In this section, we discuss the effect of including information from RSDs in the power spectrum analysis. We remind here that we restrict our analysis to the linear regime, while we do not attempt to include the non-linear distortions taking place on small scales. In this case, the dependence of the power spectrum on the angle between line of sight and wavenumber directions is expressed by equation (10). The inclusion of the RSDs provides additional information on the linear growth rate of perturbations. This test has been amply utilized to constrain cosmic growth from galaxy redshift surveys (e.g., Guzzo et al. 2008; Wang et al. 2010; Blake et al. 2011, and references therein). However, no evidence has been reported so far on the detection of such distortions in the clustering analysis of galaxy clusters. Also, this information has been never included so far in the derivation of forecasts on the constraining power of future cluster redshift surveys.

In Fig. 8, we show constraints on the  $(w_0, w_a)$  DE EoS parameters obtained by either including (blue dotted ellipse) or excluding (dot-dashed cyan ellipse) RSDs information in the analysis of the cluster power spectrum. Both contours represent constraints derived by combining the power spectrum Fisher Matrix from the combination of the three surveys, also including Planck prior on cosmological parameters and *strong prior* on mass parameters. Quite remarkably, by including information from RSDs DE constraints are tightened significantly, thanks to the additional constraints provided on the linear perturbation growth rate. This leads to an increase of the FoM by a factor of 2.2. By analysing the three surveys separately, if we do not add Planck prior, we find

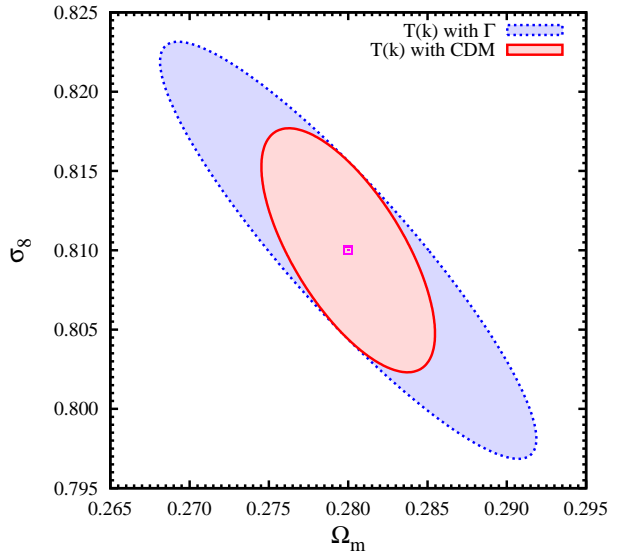


**Figure 7.** Constraints at the 68 per cent confidence level on the  $(\Omega_m, \sigma_8)$  parameters by leaving the shape parameter  $\Gamma$  as a free fitting parameter (dotted blue ellipse) or assuming its CDM dependence on  $\Omega_m, h$  and  $\Omega_b$  (solid red ellipse). All constraints are obtained by combining information from the three surveys together, including number counts and power spectrum. In both cases, we assume here the values of the parameters  $h, \Omega_b$  and  $n_s$  to be fixed at their reference values (see text). No Planck prior are assumed in this case, while *strong priors* are assumed on the mass parameters.

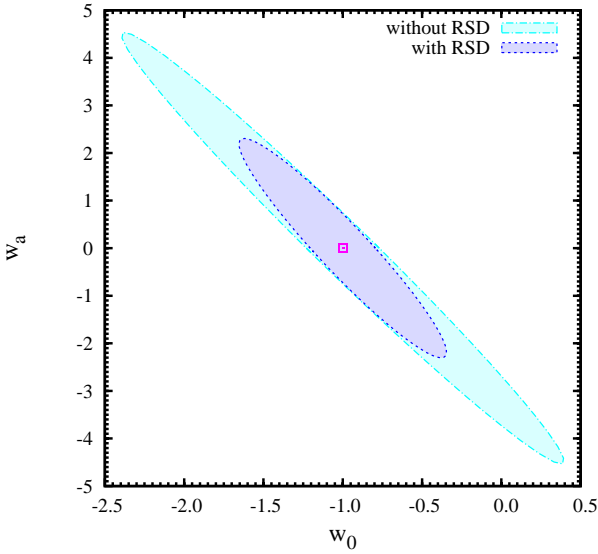


**Figure 8.** Constraints at the 68 per cent confidence level on the  $(w_0, w_a)$  DE EoS parameters, after including (dotted blue curve) or excluding (dot-dashed cyan curve) information from redshift space distortions in the cluster power spectrum analysis. The constraints are obtained by combining information for the three surveys together, including the prior information from the CMB Planck experiment, and assuming *strong prior* on the mass parameters.

that including RSDs information enhances the value of the FoM by a factor of about 35, 7.75 and 6.8 for the Wide, Medium and Deep surveys, respectively. The increasing contribution of RSDs with survey depth is due to the fact that tighter constraints are obtained by extending the redshift baseline over which the evolution of perturbation growth is followed.

We emphasize once again that large surveys of galaxy clusters do have the potential of conveying cosmological information from RSDs. This emphasizes the importance of obtaining precise redshift measurements for all clusters included in the survey.

### 3.3.6 Constraints on Early DE models

As a final analysis, we derive now forecasts for the constraints on the parameters defining the EoS of Early Dark Energy (EDE) model of equation (2), which assumes the parametrization by Grossi et al. (2009). In Fig. 9 and 10, we show constraints obtained on the  $(w_0, \Omega_{e,de})$  parameters. Cluster number counts and bias are computed by using the standard mass function by Jenkins et al. (2001). As discussed by Grossi et al. (2009), the expression of the mass function calibrated on N-body simulation according to  $\Lambda$ CDM model is also a reliable description of the one provided by simulations of EDE models, at least as long as DE is homogeneous on small scales (see also Francis et al. 2009).

Fig. 9 presents the constraints obtained for each of the three surveys and for their combination. They are obtained by combining cluster number counts and power spectrum information. We include constraints from the Planck prior and assume *strong prior* on mass parameters. The results shown in this figure confirm that the Medium survey is the one carrying most of the information on the

DE EoS. Thus we can extend to EDE models what we found in the right panel of Fig. 4 for models of equation 1 where DE influences the cosmic evolution at lower redshift. Even if the Deep survey should be more sensitive to the EDE thanks to the large number of clusters at  $z > 0.8$ , a higher FoM is found for the Medium survey. This is mainly triggered by the number of total clusters provided by the Medium survey even at high redshifts.

In order to analyse the origin of the constraints on EDE parameters, we show in Fig. 10 how such constraints are progressively tightened as we add information from cluster power spectrum and Planck experiment to the cluster number counts. The latter are expected to provide rather degenerate constraints on  $(w_0, \Omega_{e,de})$ , which is basically associated to the freedom of choosing a generic geometry of the Universe. The power spectrum analysis brings in addition both information on geometry through the shape of the transfer function and extra information on perturbation growth through RSDs. It is well known that the primary CMB, with the exception of the integrated Sachs-Wolfe effect, does not provide constraints on the dark energy for a non-flat Universe (Albrecht et al. 2006; Bean et al. 2001). However, the  $\Omega_m$  parameter is strongly constrained by the CMB and this in turn tightens the cluster constrains on DE, as we point out in Section 3.3.2 (see also Figs. 6). Furthermore, adding constraints expected from the Planck experiment causes also EDE constraints to be much improved, while changing the degeneracy direction. The reason for this is that in the EDE scenario, the purely geometrical constraints from CMB anisotropies become slightly more important due to a non-negligible DE contribution to the total energy density of the Universe at  $z \sim 10^3$ . The FoM derived from our constraints increases by a factor of 27 when we add information from the Planck experiment to the clusters analysis. In general, this further highlights that tracing cosmic growth over the widest possible range of redshift is required in order to tightly constrain the values of DE EoS parameters (Xia & Viel 2009).

## 4 CONCLUSIONS

In this paper, we presented forecasts on the capability of future wide-area high-sensitivity X-ray surveys of galaxy clusters to yield constraints on the parameters defining Dark Energy (DE) equation of states. We considered the standard equation of state (EoS) provided by equation (1) and the class of Early DE models of equation (2). Our analysis was carried out for future X-ray surveys which have enough sensitivity to provide accurate measurements of X-ray mass proxies and Fe-line based redshifts for approximately  $2 \times 10^4$  clusters, thus extending by more than two orders of magnitude the size of the cluster samples presently used to derive cosmological constraints (e.g., Allen et al. 2011). We used the Wide Field X-ray Telescope (WFXT) (e.g., Giacconi et al. 2009; Murray & WFXT Team 2010; Rosati et al. 2011) as a reference mission concept along with the Wide (20000 sq.deg.), Medium (3000 sq.deg.) and Deep (100 sq.deg.) survey configurations (see Table 1). We based our analysis on the Fisher Matrix formalism, by combining information on the cluster number counts and power spectrum, also including the effect of linear redshift-space distortions (RSDs). This analysis has been carried out with the main purpose of dissecting the cosmological information provided by geometrical and growth tests, which are both included in the analysis of number counts and clustering of galaxy clusters. The main results of this study can be summarized as follows.

- (a) When constraining the parameters of the DE EoS of equation

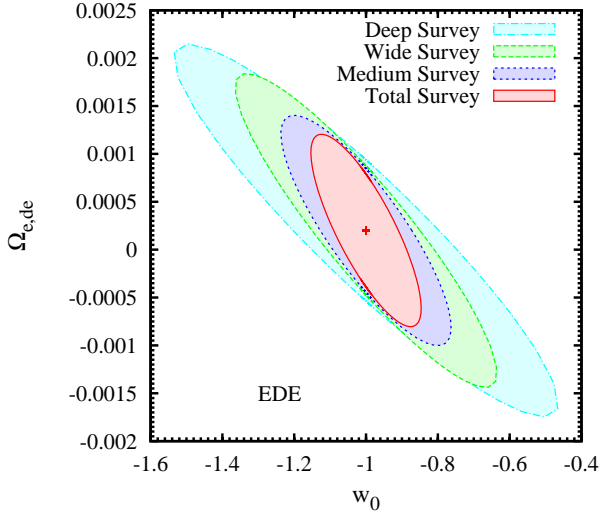


**Figure 9.** Constraints at the 68 per cent confidence level on Early Dark Energy (EDE) EoS parameters from the Deep, Medium and Wide surveys (dot-dash cyan, dotted blue and dashed green curves, respectively), by combining number counts and power spectrum information. The solid red ellipse corresponds to constraints obtained from the combination of the three surveys. The Fisher Matrix from Planck experiment and *strong prior* on mass parameters are included in the calculation of all constraints.

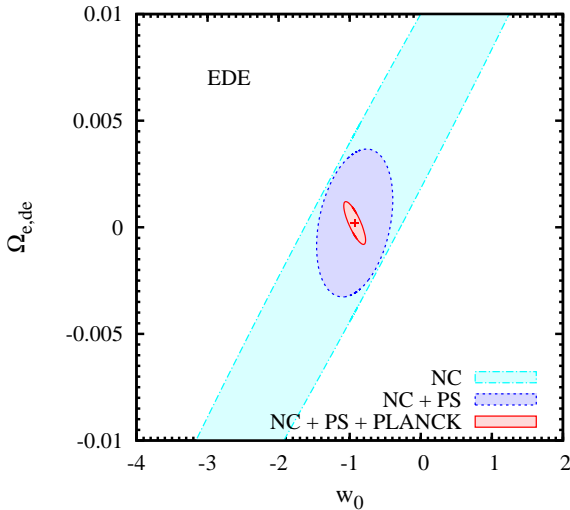


**Figure 10.** Constraints at the 68 per cent confidence level on Early Dark Energy (EDE) EoS parameters including the Fisher Matrix from number counts of cluster (dot-dashed cyan curve), adding power spectrum (dotted blue curve) and adding prior from Planck experiment (solid red curve). All constraints are obtained by combining information for the three surveys together and assuming *strong prior* on mass parameters.

(1), we further demonstrate the fundamental importance of having a well calibrated X-ray observable-mass relation and, most importantly, its redshift evolution.

We verify that the Figure of Merit (FoM) of the DE EoS increases up to 106 when we assume a strong prior on the mass parameters, as resulting from a precise and robust calibration of the mass-observable relation, with respect to the case in which no such prior is available (FoM = 61) (see Table (2)). Such an internal calibration can be readily achieved from the same X-ray data by having at least  $\sim 10^3$  net photon counts for each cluster included in the survey.

(b) We find that the Medium survey is the one carrying most of the constraining power (Table (3)), since it is expected to yield the largest number of clusters out to redshift  $z \sim 1$ . As such, the Medium survey shows the tightest constraints on the evolution of the DE EoS ( $\sigma_{w_0} = 0.097$  and  $\sigma_{w_a} = 0.54$ ) and the corresponding highest Figure of Merit (FoM = 60). The Deep survey, although covering a much smaller area than the Wide survey, adds an important contribution to constraining DE parameters (FoM = 20).

(c) We quantify the increase of the constraining power from the three surveys separately and from their combination, by adding progressively information from the cluster number counts, the mean cluster power spectrum analysis and the CMB prior from Planck experiment. We summarize in Fig. 11 the resulting improvements on FoM. The slightly different directions of degeneracy of the constraints in the  $(w_0, w_a)$  parameter space from cluster number counts and power spectrum explain why the constraints substantially improve when we consider the two contribution together rather than separately. We verified that adding the CMB information improve the corresponding constraints on the DE EoS, mostly as a consequence of the constraint provided by CMB data on the geometry of the Universe (right panel of Fig. 6).

(d) We find that RSDs carry important cosmological information through the linear growth of perturbations, also in the case of cluster surveys. Indeed, the DE FoM from the power spectrum analysis of the Wide survey increases by a factor 35 when including RSDs, while increasing by a factor 7.7 and 6.8 for the Medium and the Deep surveys, respectively.

(e) As for the information carried by the shape of the power spectrum, a smaller increase in the FoM is instead measured when including BAOs. In this case the FoM from the power spectrum analysis of the Wide survey increases by a factor of 2, while no significant information on BAOs is provided by the Medium and the Deep surveys. Furthermore, relaxing the assumption of CDM and treating the shape of the power spectrum as a free parameter reduces the FoM by a factor of 1.7 in the analysis of the Wide survey.

(f) The results obtained for the EDE EoS analysis confirm that the Medium survey is the one carrying most of the information on the DE EoS. This emphasizes once more the importance of finding a good balance in the definition of a survey strategy, between the redshift range needed to trace cosmic growth and the survey area. By extending the redshift range of the sample and with the ability to internally calibrate the observable-mass relation, we expect to measure the EDE EoS parameter ( $\Omega_{e,de}$ ) with an uncertainty of  $\sigma_{\Omega_{e,de}} = 6.6 \times 10^{-4}$ .

In order to compare the constraints from the WFXT cluster surveys to those expected from other cosmological experiments, we also compare in Fig. 11 the FoM expected from WFXT to those presented by Albrecht et al. (2006) for different large-scale structure probes. In the DETF report, they showed that Stage II cluster projects (ongoing surveys) provide FoM  $\sim 2$  (Fig. 11) when combined with Planck priors. This analysis was carried out for a generic

cluster count survey covering  $200 \text{ deg}^2$  up to  $z_{\text{max}} = 2$ , with the simple assumption of a constant mass selection function. According to Stage IV future experiments, by extending the survey area to  $20000 \text{ deg}^2$ , the FoM rises in the optimistic configuration <sup>5</sup> up to  $\sim 40$  with the contribution of the CMB Planck priors. We point out that the DETF analysis did not include the constraints expected from the power spectrum analysis. A similar value of the FoM was also obtained from an optimistic version of Stage IV project for BAO analysis based on galaxy redshift surveys, again including Planck priors. The constraining power of these optimistic <sup>6</sup> Stage IV experiments is somewhat weaker than that of the WFXT surveys, with the latter having a FoM larger by a factor of  $\gtrsim 2$ . In Fig. 11, we also show for reference the FoM expected for an optimistic <sup>7</sup> Stage IV Weak Lensing experiment, which should reach a value of about 300.

We stress that the above forecasts from the WFXT surveys are obtained by considering a subsample of clusters with at least 1500 net photon counts. With this restriction robust mass and Fe-line based redshift measurements can be readily available from the same survey data, without resorting to external follow-up calibrations or observations. As such, the derived constraints should be considered as rather conservative since they do not include possible information carried by clusters detected with a smaller number of photons or any other information to constrain mass from external observations (e.g., Sunyaev-Zeldovich fluxes, weak lensing masses and optical richness from future surveys). Lowering the flux limits of the WFXT surveys by a factor of 30 would still guarantee detection of clusters as extended sources, without however allowing a measurement of redshifts and robust mass proxies. Fig. 11 shows that by including all the detectable clusters, the FoM increases by about one order of magnitude, even by assuming no prior on the mass parameters to compensate for the lack of robust mass measurements. We note that the Wide survey provides the largest constraining power for the DE parameters when we include all clusters down to the detection limit. In fact, in this case the Wide survey dominates the statistics of clusters counts out to redshift 1.5 (see Figure 3 in Sartoris et al. (2010)). Clearly, the results obtained from all the detected clusters must be considered as optimistic, since they rely on the possibility of confirming all these extended sources and measuring their redshifts with the aid of large follow-up observations.

In general, our analysis emphasizes that for large cluster surveys to be really useful for cosmological applications, not only large samples are needed but also a robust measurement of mass proxies is required for a significant fraction of the cluster sample.

<sup>5</sup> As for the clusters analysis, according to the optimistic configuration, the mean of the mass-observable relation and its variance per redshift interval of  $\Delta z = 0.1$  is assumed in the DETF report to be determined up to a level of 1.6%.

<sup>6</sup> As for the BAOs analysis, the DETF report introduces the  $\sigma_F$  parameter, which describes the scatter in the relation between the true and the photometric redshifts,  $\sigma_F^2 = \text{Var}(z - z_{\text{phot}})/(1+z)^2$ . In the the optimistic configuration  $\sigma_F = 0.01$ .

<sup>7</sup> As for the WL analysis in the DETF report, the r.m.s. bias  $\sigma_{\ln(1+z)}$  between the mean  $z$  and photometric redshift for galaxies in  $\ln(1+z)$  for each bin of width 0.15 is assumed to be determined with a precision of 0.001. Moreover, the shear measurement is assumed to be miscalibrated by a factor  $(1 + f_{\text{cal}})$  that varies independently for each redshift bin. It is assumed that the calibration factor of each redshift bin has a Gaussian prior of width  $\sigma(f_{\text{cal}})$ . In the optimistic scenario this parameter was fixed to  $\sigma(f_{\text{cal}}) = 0.001$ .

This will be possible with future X-ray surveys only with an adequate combination of survey area, sensitivity and angular resolution. Furthermore, our results also indicates that the optimization of the survey strategy depends on the class of cosmological models that one wants to constrain. For instance, in our previous analysis presented in Sartoris et al. (2010), we showed that the Wide survey is best suited to constrain deviations from non-Gaussian initial conditions, due to its ability to sample the long wavelength modes thus detecting a possible scale-dependence of the bias. This differs from the conclusion reached in the analysis presented here, where instead we conclude that the Medium survey is best suited to trace the growth history of perturbation over a large redshift baseline, as required to follow the redshift dependence of the DE EoS. As already mentioned in the introduction, models of modified gravity and of clustered DE represent an other broad class of models for which clusters can provide important constraints (e.g., Rapetti et al. 2009; Schmidt et al. 2009; Lombriser et al. 2010). General predictions of these models are the scale-dependence of the growth factor of perturbations and of the bias function (e.g., Parfrey et al. 2011). Large cluster surveys, such as those considered in this paper, have the potential of placing important constraints on such signatures of deviations from standard quintessence variants of  $\Lambda$ CDM, especially once a suitable survey strategy is chosen.

The upcoming results from the Planck mission will much improved CMB priors based on experimental data. At the same time, the eROSITA satellite will provide in few years a wealth of fresh X-ray view of the large scale distribution of galaxy clusters and the evolution of their population out to  $z \sim 1$ . While waiting for a first X-ray satellite optimized for surveys, such as WFXT, there is no doubt that an extensive follow-up campaign will be required to provide a robust mass calibration with independent methods for a significant fraction of eROSITA clusters, so as to fully exploit the cosmological information contained in such surveys.

## ACKNOWLEDGEMENTS.

We acknowledge useful discussions with Pierluigi Monaco, Anais Rassat and with all members of the WFXT team. This work has been partially supported by the PRIN-INAF 2009 Grant ‘‘Towards an Italian Network for Computational Cosmology’’, by the European Commission’s Framework Programme 7, through the Marie Curie Initial Training Network CosmoComp (PITN-GA-2009-238356), by the PRIN/MIUR-2009 grant ‘‘Tracing the growth of structures in the Universe’’ and by the PD51 INFN Grant. BS and SB acknowledge the hospitality of the Kavli Institute for Theoretical Physics, where part of this work has been carried out. This research was supported in part by the National Science Foundation under Grant No. NSF PHY05-51164. We also acknowledge support from the DFG cluster of excellence Origin and Structure of the Universe.

## REFERENCES

- Abramo L. R., 2011, ArXiv e-prints, 1108.5449  
 Alam U., Lukić Z., Bhattacharya S., 2011, ApJ, 727, 87  
 Albrecht A., Amendola L., Bernstein G., Clowe D., Eisenstein D., Guzzo L., Hirata C., Huterer D., Kirshner R., Kolb E., Nichol R., 2009, ArXiv e-prints, 0901.0721

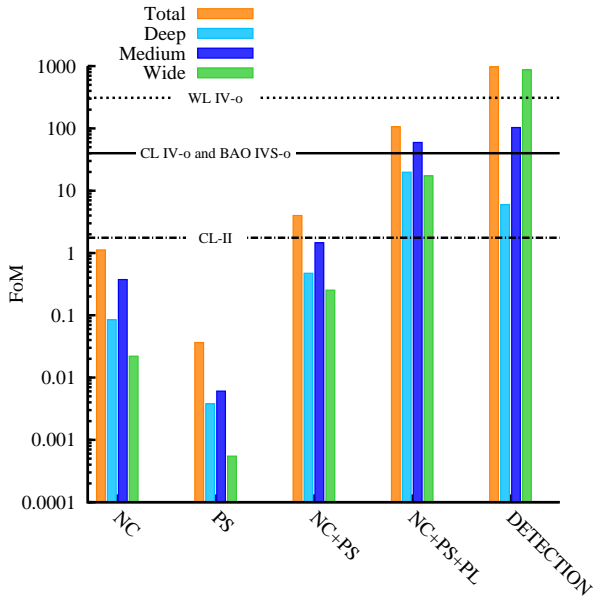


**Figure 11.** The histograms represent the Figures of Merit for the  $(w_0, w_a)$  parameters from WFXT surveys, as derived in the following configurations: by including in the Fisher Matrix the cluster number counts only (NC), the cluster mean power spectrum only (PS), the sum of the two (NC+PS), and by adding the prior from the Planck experiment (NC+PS+PL). All these FoM are obtained by assuming *strong prior* on mass parameters. The last group of histograms shows FoMs as obtained in the configuration NC+PS+PL by considering all clusters that can be detected ( $\approx 30$  source counts) in a given survey and by assuming *no prior* on mass parameters. The FoM for the Deep the Medium and the Wide cluster surveys are shown with the cyan, blue, green histograms respectively. The yellow histogram represent the FoM obtained from the combination of the three surveys. The horizontal lines show the FoM as reported in the DETF (Albrecht et al. 2006) for Stage II Cluster projects (CL-II; dot-dashed), for optimistic Stage IV BAO and Cluster projects (BAO IVS-o and CL IVS-o, respectively; solid line) and for optimistic Stage IV Weak Lensing project (WL IV-o; dotted line), by combining each probe with CMB Planck priors.

Albrecht A., Bernstein G., Cahn R., Freedman W. L., Hewitt J., Hu W., Huth J., Kamionkowski M., Kolb E. W., Knox L., Mather J. C., Staggs S., Sutzteff N. B., 2006, ArXiv e-prints, 0609591  
 Allen S. W., Evrard A. E., Mantz A. B., 2011, ArXiv e-prints, 1103.4829  
 Amendola L., 2000, Phys. Rev. D, 62, 043511  
 Appleby S. A., Battye R. A., Starobinsky A. A., 2010, JCAP, 6, 5  
 Balaguera-Antolínez A., Sánchez A. G., Böhringer H., Collins C., Guzzo L., Phleps S., 2011, MNRAS, pp 139–+  
 Basilakos S., Plionis M., Lima J. A. S., 2010, Phys. Rev. D, 82, 083517  
 Battye R. A., Weller J., 2003, Phys. Rev. D, 68, 083506  
 Bean R., Hansen S. H., Melchiorri A., 2001, Phys. Rev. D, 64, 103508  
 Bento M. C., Bertolami O., Sen A. A., 2002, Phys. Rev. D, 66, 043507  
 Blake C., Brough S., Colless M., Contreras C., Couch W., Croom S., Davis T., Drinkwater M. J., et al. 2011, MNRAS, 415, 2876  
 Böhringer H., Schuecker P., Guzzo L., Collins C. A., Voges W., Cruddace R. G., Ortiz-Gil A., Chincarini G., De Grandi S., Edge A. C., MacGillivray H. T., Neumann D. M., Schindler S., Shaver

P., 2004, A&A, 425, 367  
 Borgani S., Kravtsov A., 2009, ArXiv e-prints, 0906.4370  
 Brax P., van de Bruck C., Davis A.-C., Shaw D. J., 2008, Phys. Rev. D, 78, 104021  
 Caldwell R. R., Kamionkowski M., 2009, Annual Review of Nuclear and Particle Science, 59, 397  
 Chevallier M., Polarski D., 2001, International Journal of Modern Physics D, 10, 213  
 Corasaniti P. S., Copeland E. J., 2003, Phys. Rev. D, 67, 063521  
 Crocce M., Scoccimarro R., 2008, Phys. Rev. D, 77, 023533  
 Cunha C., 2009, Phys. Rev. D, 79, 063009  
 Cunha C. E., Evrard A. E., 2010, Phys. Rev. D, 81, 083509  
 Dodelson S., 2003, Modern cosmology  
 Doran M., Wetterich C., 2003, Nuclear Physics B Proceedings Supplements, 124, 57  
 Dvali G., Gabadadze G., Porrati M., 2000, Physics Letters B, 485, 208  
 Ebeling H., Edge A. C., Böhringer H., Allen S. W., Crawford C. S., Fabian A. C., Voges W., Huchra J. P., 1998, MNRAS, 301, 881  
 Ebeling H., Edge A. C., Mantz A., Barrett E., Henry J. P., Ma C. J., van Speybroeck L., 2010, MNRAS, 407, 83  
 Eisenstein D. J., Hu W., 1998, ApJ, 496, 605  
 Fabjan D., Borgani S., Rasia E., Bonafede A., Dolag K., Murante G., Tornatore L., 2011, MNRAS, 416, 801  
 Feldman H. A., Kaiser N., Peacock J. A., 1994, ApJ, 426, 23  
 Francis M. J., Lewis G. F., Linder E. V., 2009, MNRAS, 393, L31  
 Gehrels N., 1986, ApJ, 303, 336  
 Giacconi R., Borgani S., Rosati P., Tozzi P., Gilli R., et al. 2009, in AGB Stars and Related Phenomena2010: The Astronomy and Astrophysics Decadal Survey Vol. 2010 of Astronomy, Galaxy clusters and the cosmic cycle of baryons across cosmic times. pp 90–+  
 Grossi M., Springel V., 2009, MNRAS, 394, 1559  
 Grossi M., Verde L., Carbone C., Dolag K., Branchini E., Iannuzzi F., Matarrese S., Moscardini L., 2009, MNRAS, 398, 321  
 Guzzo L., Pierleoni M., Meneux B., Branchini E., Le Fèvre O., et al. 2008, Nature, 451, 541  
 Hannestad S., 2010, Progress in Particle and Nuclear Physics, 65, 185  
 Holder G., Haiman Z., Mohr J. J., 2001, ApJ, 560, L111  
 Hu W., Sawicki I., 2007, Phys. Rev. D, 76, 064004  
 Jenkins A., Frenk C. S., White S. D. M., Colberg J. M., Cole S., Evrard A. E., Couchman H. M. P., Yoshida N., 2001, MNRAS, 321, 372  
 Kaiser N., 1987, MNRAS, 227, 1  
 Komatsu E., Smith K. M., Dunkley J., Bennett C. L., Gold B., Hinshaw G., Jarosik N., Larson D., Nolte M. R., Page L., et al. 2011, ApJS, 192, 18  
 Kravtsov A. V., Vikhlinin A., Nagai D., 2006, ApJ, 650, 128  
 Larson D., Dunkley J., Hinshaw G., Komatsu E., Nolte M. R., Bennett C. L., Gold B., Halpern M., Hill R. S., Jarosik N., et al. 2011, ApJS, 192, 16  
 Lima M., Hu W., 2005, Phys. Rev. D, 72, 043006  
 Lima M., Hu W., 2007, Phys. Rev. D, 76, 123013  
 Linder E. V., 2003, Physical Review Letters, 90, 091301  
 Lombriser L., Slosar A., Seljak U., Hu W., 2010, ArXiv e-prints  
 Mahdavi A., Hoekstra H., Babul A., Henry J. P., 2008, MNRAS, 384, 1567  
 Majumdar S., Mohr J. J., 2003, ApJ, 585, 603  
 Majumdar S., Mohr J. J., 2004, ApJ, 613, 41  
 Manera M., Mota D. F., 2006, MNRAS, 371, 1373

- Mantz A., Allen S. W., Ebeling H., Rapetti D., Drlica-Wagner A., 2009, ArXiv e-prints, 0909.3099
- Mantz A., Allen S. W., Rapetti D., 2010, MNRAS, 406, 1805
- Mantz A., Allen S. W., Rapetti D., Ebeling H., 2010, MNRAS, 406, 1759
- Marriage T. A., the ACT Team 2011, ApJ, 737, 61
- Marulli F., Carbone C., Viel M., Moscardini L., Cimatti A., 2011, ArXiv e-prints, 1103.0278
- Maughan B. J., 2007, ApJ, 668, 772
- Movahed M. S., Farhang M., Rahvar S., 2009, International Journal of Theoretical Physics, 48, 1203
- Mukohyama S., Randall L., 2004, Physical Review Letters, 92, 211302
- Murray S. S., WFXT Team 2010, in Bulletin of the American Astronomical Society Vol. 41 of Bulletin of the American Astronomical Society, The Wide Field X-ray Telescope Mission. pp 520–+
- Okabe N., Zhang Y., Finoguenov A., Takada M., Smith G. P., Umetsu K., Futamase T., 2010, ApJ, 721, 875
- Parfrey K., Hui L., Sheth R. K., 2011, Phys. Rev. D, 83, 063511
- Percival W. J., White M., 2009, MNRAS, 393, 297
- Perlmutter S., Aldering G., Goldhaber G., Knop R. A., Nugent P., Castro P. G., Deustua S., Fabbro S., The Supernova Cosmology Project 1999, ApJ, 517, 565
- Planck Collaboration 2011, ArXiv e-prints, 1101.2024
- Predehl P., Andritschke R., Bornemann W., Bräuninger H., Briel U., et al. 2007, in Society of Photo-Optical Instrumentation Engineers (SPIE) Conference Series Vol. 6686 of Society of Photo-Optical Instrumentation Engineers (SPIE) Conference Series, eROSITA
- Rapetti D., Allen S. W., Mantz A., Ebeling H., 2009, MNRAS, 400, 699
- Rapetti D., Allen S. W., Weller J., 2005, MNRAS, 360, 555
- Rassat A., Amara A., Amendola L., Castander F. J., Kitching T., Kunz M., Refregier A., Wang Y., Weller J., 2008, ArXiv e-prints, 0810.0003
- Ratra B., Peebles P. J. E., 1988, Phys. Rev. D, 37, 3406
- Reid B. A., Percival W. J., Eisenstein D. J., Verde L., Spergel D. N., Skibba R. A., Bahcall N. A., Budavari T., et al. 2010, MNRAS, 404, 60
- Riess A. G., Strolger L.-G., Casertano S., Ferguson H. C., Mobasher B., Gold B., Challis P. J., Filippenko A. V., et al. 2007, ApJ, 659, 98
- Rosati P., Borgani S., Gilli R., Paolillo M., Tozzi P., Murray S., Giacomini R., Ptak A., Weisskopf M., Forman W., Jones C., WFXT Team 2011, Memorie della Societa Astronomica Italiana Supplementi, 17, 8
- Rosati P., Borgani S., Norman C., 2002, ARAA, 40, 539
- Rosati P., della Ceca R., Norman C., Giacomini R., 1998, ApJ, 492, L21+
- Sartoris B., Borgani S., Fedeli C., Matarrese S., Moscardini L., Rosati P., Weller J., 2010, MNRAS, 407, 2339
- Schmidt F., Vikhlinin A., Hu W., 2009, Phys. Rev. D, 80, 083505
- Sheth R. K., Tormen G., 1999, MNRAS, 308, 119
- Silvestri A., Trodden M., 2009, Reports on Progress in Physics, 72, 096901
- Skordis C., 2009, Classical and Quantum Gravity, 26, 143001
- Sotiriou T. P., Faraoni V., 2010, Reviews of Modern Physics, 82, 451
- Stanek R., Rasia E., Evrard A. E., Pearce F., Gazzola L., 2010, ApJ, 715, 1508
- Staniszewski Z., Ade P. A. R., Aird K. A., Benson B. A., Bleem L. E., Carlstrom J. E., Chang C. L., Cho H.-M. e., 2009, ApJ, 701, 32
- Stril A., Cahn R. N., Linder E. V., 2010, MNRAS, 404, 239
- Tegmark M., 1997, Physical Review Letters, 79, 3806
- Tinker J., Kravtsov A. V., Klypin A., Abazajian K., Warren M., Yepes G., Gottlöber S., Holz D. E., 2008, ApJ, 688, 709
- Truemper J., 1993, Science, 260, 1769
- TsujiKawa S., 2010, ArXiv e-prints, 1004.1493
- Vikhlinin A., Burenin R. A., Ebeling H., Forman W. R., Hornstrup A., Jones C., Kravtsov A. V., Murray S. S., Nagai D., Quintana H., Voevodkin A., 2009, ApJ, 692, 1033
- Vikhlinin A., Kravtsov A. V., Burenin R. A., Ebeling H., Forman W. R., Hornstrup A., Jones C., Murray S. S., Nagai D., Quintana H., Voevodkin A., 2009, ApJ, 692, 1060
- Wang Y., Percival W., Cimatti A., Mukherjee P., Guzzo L., Baugh C. M., Carbone C., Franzetti P., Garilli B., Geach J. E., Lacey C. G., Majerotto E., Orsi A., Rosati P., Samushia L., Zamorani G., 2010, MNRAS, 409, 737
- Wetterich C., 2004, Physics Letters B, 594, 17
- Williamson R., the SPT Team 2011, ApJ, 738, 139
- Xia J.-Q., Viel M., 2009, JCAP, 4, 2
- Yu H., Tozzi P., Borgani S., Rosati P., Zhu Z.-H., 2011, A&A, 529, A65+
- Zhang Y.-Y., Okabe N., Finoguenov A., Smith G. P., Piffaretti R., Valdarnini R., Babul A., Evrard A. E., Mazzotta P., Sanderson A. J. R., Marrone D. P., 2010, ApJ, 711, 1033
- Zlatev I., Wang L., Steinhardt P. J., 1999, Physical Review Letters, 82, 896